RESEARCH ARTICLE

A tripole pattern of summer surface air temperature anomalies over northern Eurasia and its precursory signals in the tropical Atlantic and northern Asian land

Kejun He[1] 🅘 | Ge Liu[1,2] 🅘 | Renguang Wu[3] 🅘 | Jingxin Li[1] | Huimei Wang[1] | Xiaoyuan Yue[1]

[1]State Key Laboratory of Severe Weather, Chinese Academy of Meteorological Sciences, Beijing, China

[2]Collaborative Innovation Centre on Forecast and Evaluation of Meteorological Disasters, Nanjing University of Information Science and Technology, Nanjing, China

[3]Department of Atmospheric Sciences, School of Earth Sciences, Zhejiang University, Hangzhou, China

Correspondence
Ge Liu, State Key Laboratory of Severe Weather, Chinese Academy of Meteorological Sciences, 46 Zhong-Guan-Cun South Avenue, Beijing 100081, China.
Email: liuge@cma.gov.cn

Funding information
The Basic Research Fund of CAMS, Grant/Award Number: Grant 2019Z008; The National Key Research and Development Program of China, Grant/Award Number: Grant 2018YFC1507102; The Science and Technology Development Fund of CAMS, Grant/Award Number: Grant 2019KJ022; The Second Tibetan Plateau Scientific Expedition and Research (STEP) program, Grant/Award Number: 2019QZKK0105; The Strategic Priority Research Program of the Chinese Academy of Sciences, Grant/Award Number: Grant XDA20100300

Abstract

This study investigates the variability of summer surface air temperature (SAT) over northern Eurasia and its precursory signals in the tropical Atlantic and northern Asian land. The leading mode of summer SAT variations features a northern Eurasian SAT tripole (NEST) pattern, with two same-sign SAT anomaly regions over eastern Europe–western Siberia and the Far East region and an opposite-sign SAT anomaly region around the Baikal Lake. It is found that sea surface temperature (SST) or SAT anomalies in the tropical Atlantic and rainfall-soil moisture anomalies around the Baikal Lake during May can modulate the NEST pattern. The SST anomalies in the tropical Atlantic persist from May to summer and induce a downstream zonal wave train across northern Eurasia, consequently causing the variation in the summer NEST pattern. May rainfall anomalies around the Baikal Lake affect the overlying atmospheric circulation during summer through the 'memory' effect of soil moisture and the soil moisture-rainfall interaction, correspondingly modulating the downstream wave train and the associated NEST pattern. Based on the above results, a statistical prediction model is established using the two precursory signals, that is, SAT in the tropical Atlantic and rainfall around the Baikal Lake during May. The leave-three-out cross-validation shows that the model has a high skill in predicting the summer NEST pattern, with a correlation coefficient of 0.51 (significant at the 99.8% confidence level) between observation and prediction during the period 1980–2016.

KEYWORDS

Eurasia, prediction, soil moisture, surface air temperature, the Atlantic Ocean

1 | INTRODUCTION

Summer SAT anomalies over Eurasia have an important influence on the economic and social development and lives of people in the region. For instance, extremely high

SAT anomalies in western and central Europe caused wildfires and severe economic losses during the summer of 2003 (Beniston, 2004; Stott *et al.*, 2004). An unprecedented high SAT event (heatwave) struck Russia and resulted in severe forest fires and crop failures during the

summer of 2010 (Barriopedra *et al.*, 2011; Sedláček *et al.*, 2011). Low SAT anomalies during the warm season can also damage crops at high latitudes (Ma *et al.*, 2003; Fang *et al.*, 2005). In addition to these local and direct impacts, the SAT anomalies may also change the land-sea thermal contrast between Eurasian and the Pacific and therefore affect the variability of the Asian summer monsoon (Liu and Yanai, 2001; D'Arrigo *et al.*, 2006). Thus, it is of great importance to explore the variability of summer SAT over Eurasia and its precursory factors and to understand associated physical mechanisms. This may favour the socioeconomic development over both local regions and broader Asian monsoon areas.

Land and oceanic conditions are considered as crucial factors affecting Eurasian SAT. Local soil–atmosphere feedbacks play important roles in driving regional temperature extremes over Europe (Fischer *et al.*, 2012; Boé and Terray, 2014; Miralles *et al.*, 2014; Whan *et al.*, 2015). Also, the soil moisture feedbacks can affect summer SAT over various areas of East Asia (Zhang and Dong, 2010). A west–east dipole pattern of spring snow cover variations over Eurasia, which may affect soil moisture during the following season, pronouncedly modulates Eurasian SAT and precipitation anomalies during spring and the subsequent summer (Wu *et al.*, 2014). In addition to the abovementioned effects of land surface forcing, sea surface temperature anomalies (SSTAs) in different oceanic regions contribute to SAT anomalies over Eurasia. Observations and numerical simulations reveal that SSTAs in the tropical Atlantic Ocean, the Mediterranean Basin, the North Sea, and further north toward the Arctic Circle, contribute to SAT anomalies in Europe (Cassou *et al.*, 2005; Sutton and Hodson, 2005; Feudale and Shukla, 2011a, 2011b). The El Niño–Southern Oscillation (ENSO) and related anomalous heating over the tropical Pacific and Atlantic can affect summer SAT over western Russia through exciting a Rossby wave extending northwestward to western Russia (Sun *et al.*, 2016). The North Atlantic SSTAs play an important role in inducing persisting atmospheric circulation pattern over Eurasia and in the maintenance of Eurasian SAT anomaly pattern from winter to spring (Wu and Chen, 2020).

Specifically, the SSTAs in the Atlantic Ocean not only influence climate anomalies in adjacent Europe (Cassou *et al.*, 2005; Sutton and Hodson, 2005, 2007; Feudale and Shukla, 2011a, 2011b; Sutton and Dong, 2012; Saeed *et al.*, 2014), but also remotely adjust, to some extent, Asian circulation and associated climate variability on different timescales (Goswami *et al.*, 2006; Lu *et al.*, 2006; Li *et al.*, 2008, 2015; Wu *et al.*, 2009; Wu *et al.*, 2010, 2011; Zuo *et al.*, 2013; Sun, 2014; Krishnamurthy and Krishnamurthy, 2016; Wang *et al.*, 2017). Therefore, attention should be paid to the contribution of the SSTAs

in the Atlantic Ocean when investigating integral structures of climate anomalies over Eurasia. For example, a tripole SSTA pattern in the North Atlantic can modulate summer SAT over Northeast China (Wu *et al.*, 2010, 2011). The tripole SSTA pattern in the North Atlantic contributes largely to SAT anomalies over mid- to high-latitude Eurasia during spring (Chen and Wu, 2017). A horseshoe-shaped SSTA pattern in the North Atlantic can stimulate wave-train-like atmospheric circulation anomalies over the North Atlantic through Eurasia, therefore contributing to a tripole anomaly pattern of SAT over Eurasia during spring (Chen *et al.*, 2016). Recent studies further revealed the impact of the Atlantic SSTAs on SAT over the Middle East and Arabian Peninsula during summer time (Ehsan *et al.*, 2019, 2020).

Given the importance of oceanic thermal and land soil moisture anomalies in modulating SAT over Eurasia, we explore precursory signals of the summer SAT anomalies over Eurasia from the underlying surface conditions, in particular, those in the Atlantic Ocean and Eurasian land. The rest of the paper is organized as follows. In Section 2, the data and methods are described. The characteristics of the variability of summer SAT over northern Eurasia and associated atmospheric circulation anomalies are presented in Section 3. Section 4 explores the simultaneous and preceding underlying surface conditions that are responsible for the summer SAT anomalies over northern Eurasia. The associated physical processes linking the preceding oceanic and land signals and summer Eurasian SAT anomalies are proposed in Section 4. Finally, a summary and discussion are given in Section 5.

2 | DATA AND METHODS

The SAT connecting with heatwaves and cold damages generally refers to that in thermometer screen at 1.5 m. Thus, this study used monthly mean air temperature at a close level (i.e., 2 m) to indicate the high-impact SAT. The 2 m air temperature, pressure-level geopotential height, U- and V-wind, and vertical velocity (omega) data, which are obtained from the National Centers for Environmental Prediction (NCEP)–National Center for Atmospheric Research (NCAR) reanalysis I (Kalnay *et al.*, 1996). The monthly mean precipitation on $2.5° × 2.5°$ grids was obtained from the Climate prediction centre (CPC) Merged Analysis of Precipitation (CMAP; Xie and Arkin, 1997). We also used monthly mean soil moisture on $0.75° × 0.75°$ grids of ERA-Interim reanalysis (Dee *et al.*, 2011) of the European Center for Medium-Range Weather Forecasts. The National Oceanic and Atmospheric Administration (NOAA) extended

reconstructed SST version 4 (Huang *et al.*, 2015) was also used. The monthly mean air temperature at 2 m and pressure-level geopotential height on $0.75° \times 0.75°$ grids of ERA-Interim reanalysis (Berrisford *et al.*, 2011) were also used to verify the results. The above data are all extracted from 1980 to 2016.

During the period 1980–2016, there are significant increasing trends in summer SAT over most regions of Eurasia (not shown), which may reflect the concurrent responses to global warming, rather than realistic intrinsic relationships. To investigate the interannual and interdecadal variability of summer SAT over Eurasia and its potential reasons, rather than the linear trend, we removed linear trends from all data used in this study.

An empirical orthogonal function (EOF) (Obukhov, 1947; Kundu and Allen, 1976) was used to acquire the dominant mode of summer SAT variation over northern Eurasia ($35°–70°$N, $20°–160°$E). In addition, wave-activity flux was used to diagnose the propagation of stationary waves. The wave activity flux **W** is expressed as follows:

$$\mathbf{W} = \frac{p}{2|\mathbf{U}|} \begin{pmatrix} U(v'^2 - \psi'v'_x) + V(-u'v' + \psi'u'_x) \\ U(-u'v' + \psi'u'_x) + V(u'^2 + \psi'u'_y) \\ \frac{f_0 R_d}{N^2 H_0}\left\{ U(v'T' - \psi'T'_x) + V(-u'T' - \psi'T'_y) \right\} \end{pmatrix},$$

where ψ' denotes perturbation geostrophic stream function, $\mathbf{u}' = (u', v')$ perturbation geostrophic wind velocities, $\mathbf{U} = (U, V)$ a horizontal basic flow velocity, p pressure normalized by 1,000 mb, R_d the gas constant of dry air, H_0 the constant scale height, f_0 the coriolis force constant at the middle latitude of $50°$N, N^2 the Brunt-Väisälä frequency and T the temperature (Takaya and Nakamura, 1997, 2001; Bueh and Nakamura, 2007). Several studies indicated that this flux can successfully capture the downstream propagation of Rossby wave energy stimulated by the Atlantic thermal anomalies (Liu *et al.*, 2012; Wang *et al.*, 2017; Yue *et al.*, 2020).

A linear fitting method was applied to show the independent effect of one factor after removing the variation of the other factor (Hu *et al.*, 2012). For the two time series X1 and X2, the X2-related variation (called X1′) of X1 can be obtained through a linear fitting method, in which the variation of X1 is regarded as a dependent variable and the variation of X2 as an independent variable. The residual of the linear fitting (i.e., the difference X1 minus X1′) can be used to reflect the individual variation of X1 independent of X2 (Yue *et al.*, 2020).

Eight-year high-/low-pass Lanczos filtering was used to extract interannual/interdecadal components from a raw variable (Duchon, 1979). Correlation, composite, and regression methods were used in this study. Unless otherwise stated, the statistical significance was evaluated using the Student′s *t* test.

Because the degrees of freedom are reduced after filtering or removing linear trends, we assessed the statistical significance using a Monte Carlo test (Besag and Clifford, 1989; Tippett, 2004; Ehsan *et al.*, 2017). For the Monte Carlo test of an EOF analysis, we randomly scrambled the order of SAT during the period 1980–2016 for 1,000 times. After removing the linear trends of SAT, the EOF analyses of random summer SAT anomalies over northern Eurasia were repeated 1,000 times. The 95th (99th) percentile value of the sorted explained variance of the leading EOF mode is considered as the threshold value of 95% (99%) confidence level. Similarly, for the Monte Carlo test of correlation between the interdecadal components (obtained using low-pass Lanczos filtering) of two time series, the order of time series was randomly scrambled and then filtered. The process was repeated 10,000 times, and the threshold for statistical significance is the 95th percentile.

We used binary linear regressions to construct a statistical prediction model of the dominant mode of summer SAT anomalies over northern Eurasia. Referring to Gao *et al.* (2018), the correlation coefficients between the observation and prediction were used to represent the skills of statistical prediction models. The skills can be tested using the method of leave-three-out cross-validation (Michaelsen, 1987).

3 | TRIPOLE PATTERN OF SUMMER SAT ANOMALIES OVER NORTHERN EURASIA AND ASSOCIATED ATMOSPHERIC CIRCULATION ANOMALIES

We performed an EOF analysis of summer SAT anomalies over northern Eurasia during the period 1980–2016 (not shown). The leading EOF mode (EOF1) accounts for 19% of the total variance, which is significant at the 99% confidence level based on 1,000-time Monte Carlo simulation (Besag and Clifford, 1989). The summer SAT anomalies regressed upon the standardized principal component (PC1) of EOF1 reveal a tripole pattern over northern Eurasia, with same-sign SAT anomalies over the eastern Europe–western Siberia region and the Far East region and opposite-sign SAT anomalies over the Baikal Lake region (Figure 1a).

For convenience, a northern Eurasian SAT tripole (NEST) index (I_{NEST}) was defined to represent the variation of this pattern. The NEST index is calculated using the following formula:
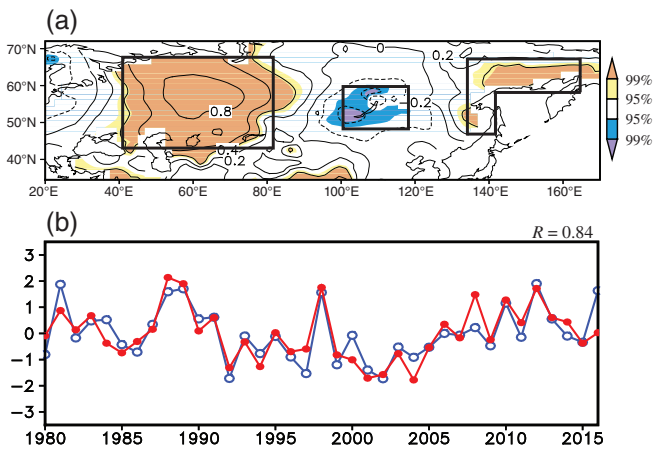
FIGURE 1 (a) Summer SAT anomalies (units: °C) regressed upon the standardized time series of principal component (PC1) of EOF1. Shadings denote SAT anomalies significant at the 95% and 99% confidence levels as shown by the colour bars. The three black boxes from left to right represent the eastern Europe–western Siberia (43°–67°N, 40°–80°E), Baikal Lake (48°–60°N, 97°–115°E) and the Far East (58°–68°N, 130°–160°E and 47°–58°N, 130°–138°E) regions, respectively. (b) Standardized time series of the summer NEST (red line) and PC1 (blue line) indices [Colour figure can be viewed at wileyonlinelibrary.com]

$$I_{NEST} = T_{EEWS} - T_{BL} + T_{FE},$$

in which T_{EEWS}, T_{BL} and T_{FE} indicate the area-mean summer SAT anomalies over the regions of eastern Europe–western Siberia (EEWS; 43°–67°N, 40°–80°E), Baikal Lake (BL; 48°–60°N, 97°–115°E) and Far East (FE; 58°–68°N, 130°–160°E and 47°–58°N, 130°–138°E), respectively (see the black boxes in Figure 1a). The T_{EEWS} has a correlation coefficient of −0.38 (0.44) with T_{BL} (T_{FE}), significant at the 95% confidence level. The significant correlations imply that the variations of summer SAT over the three regions have an intrinsic connection, leading to the tripole pattern of SAT anomalies over northern Eurasia during summer. The I_{NEST} is highly consistent with the PC1, with a correlation coefficient of 0.84, significant at the 99.9% confidence level (Figure 1b). Thus, the I_{NEST} can be used to measure the summer NEST pattern.

Summer 200-hPa geopotential height anomalies obtained by regression upon the summer NEST index (Figure 2a) show that corresponding to a higher NEST index, significant positive anomalies appear over the EEWS region and over the FE region and its adjacent Okhotsk Sea, while negative anomalies appear over the BL region. This forms a positive–negative–positive pattern. The NEST-related positive–negative–positive pattern is also observed in summer 500- and 850-hPa geopotential height anomalies (not shown), indicative of a barotropic vertical structure of geopotential height
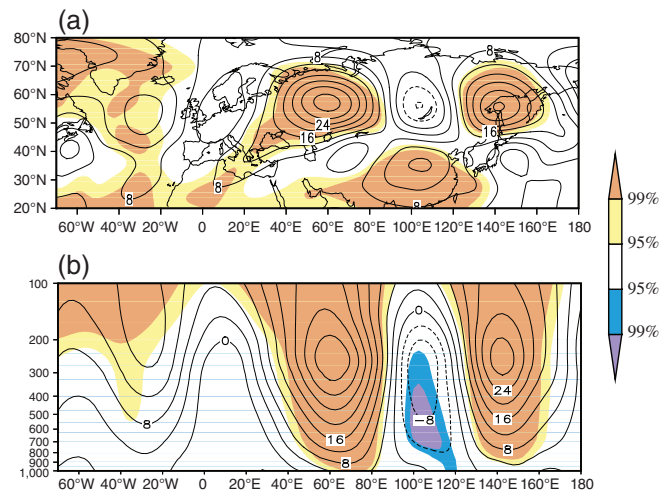

FIGURE 2 (a) Summer 200-hPa geopotential height anomalies (units: gpm) obtained by regression on the summer NEST index for the period 1980–2016. (b) As in (a) but for the zonal–vertical cross section along 55°N. Contours are drawn every 4 gpm. Shadings denote geopotential height anomalies significant at the 95% and 99% confidence levels as shown by the colour bars [Colour figure can be viewed at wileyonlinelibrary.com]

anomalies over northern Eurasia. This can also be clearly identified in geopotential height anomalies regressed upon the summer NEST index along 55°N (Figure 2b). There are deep high-pressure anomalies around 40°–80°E (the EEWS region) and 130°–160°E (the FE region), and deep low-pressure anomalies around 95°–120°E (the BL region). The deep high-pressure anomalies can reduce upward motion/rainfall, and hence increase downward solar radiation reaching the surface of the Earth, causing higher SAT over the EEWS and FE regions. In contrast, the low-pressure anomalies can lead to lower SAT over the BL region through enhancing upward motion/rainfall, and therefore decreasing downward solar radiation reaching the surface. Such a positive–negative–positive pattern of geopotential height anomalies induces the NEST pattern.

Figure 2a also shows that the positive–negative–positive pattern of geopotential height anomalies over northern Eurasia can be traced to the upstream mid- to high-latitude North Atlantic, signifying a zonal wave train extending from the Atlantic to Eurasia. Rossby wave trains from the Atlantic to Eurasia can be stimulated by SST and related SAT anomalies in the Atlantic Ocean and affect downstream climate variability over the Eurasian continent (Wu et al., 2010, 2011; Wang et al., 2017). The above results imply a potential contribution of the Atlantic thermal anomalies to the NEST pattern. Therefore, we investigate the effect of summer SST and associated SAT anomalies in the Atlantic Ocean in the following section.

4 | OCEANIC AND LAND SIGNALS CONTRIBUTING TO THE NEST ANOMALIES

4.1 | The effect of summer thermal anomalies in the tropical Atlantic

The correlation between the summer NEST index and simultaneous SAT/SST over the Atlantic Ocean is presented in Figure 3. Significant positive correlations appear over the tropical Atlantic and mid-latitude North Atlantic regions. Vertically superposed SST and SAT anomalies over the tropical Atlantic are significantly correlated with the NEST index, which implies that the SST and SAT anomalies related to the summer NEST are tightly coupled. The area-mean SAT/SST averaged over the tropical Atlantic region (0°–20°N, 80°–25°W and 0°–10°N, 25°–5°W and 35°–5°W, 10°S–0°) is referred to as the tropical Atlantic SAT/SST index. The summer tropical Atlantic SAT and SST indices are closely related to the simultaneous NEST index, with correlation coefficients of 0.59 and 0.53, respectively, both significant at the 99.9% confidence level. The two correlation coefficients also indicate that the SAT has a higher correlation with the summer NEST index over the tropical Atlantic Ocean

As such, the tropical Atlantic SAT is a better choice for investigating the SST-SAT coupled thermal effect on the summer NEST.

The summer area-mean SAT/SST averaged over the mid-latitude North Atlantic region (45°–25°W, 33°–50°N) is defined as the summer mid-latitude North Atlantic SAT/SST index, which is also significantly correlated with the summer NEST index, with a correlation coefficient of 0.58/0.48. Similarly, hereinafter we used the mid-latitude North Atlantic SAT index to represent the SST-SAT coupled thermal anomalies over this region.

Further analyses indicate that surface thermal (SST/SAT) anomalies in the tropical Atlantic, rather than those in the mid-latitude North Atlantic region, seem to excite local atmospheric circulation anomalies and may, therefore, modulate downstream circulation and related SAT anomalies over northern Eurasia. The correlation between the summer tropical Atlantic SAT index and concurrent 1,000-hPa geopotential heights (Figure 4a) is significantly negative over the tropical Atlantic Ocean. This implies that warmer (cooler) surface thermal anomalies lead to low-level lower (higher) pressure over the tropical Atlantic region. This is consistent with the response of the 'warm SST–low pressure' type revealed by Sutton and Hodson (2005). The correlation between
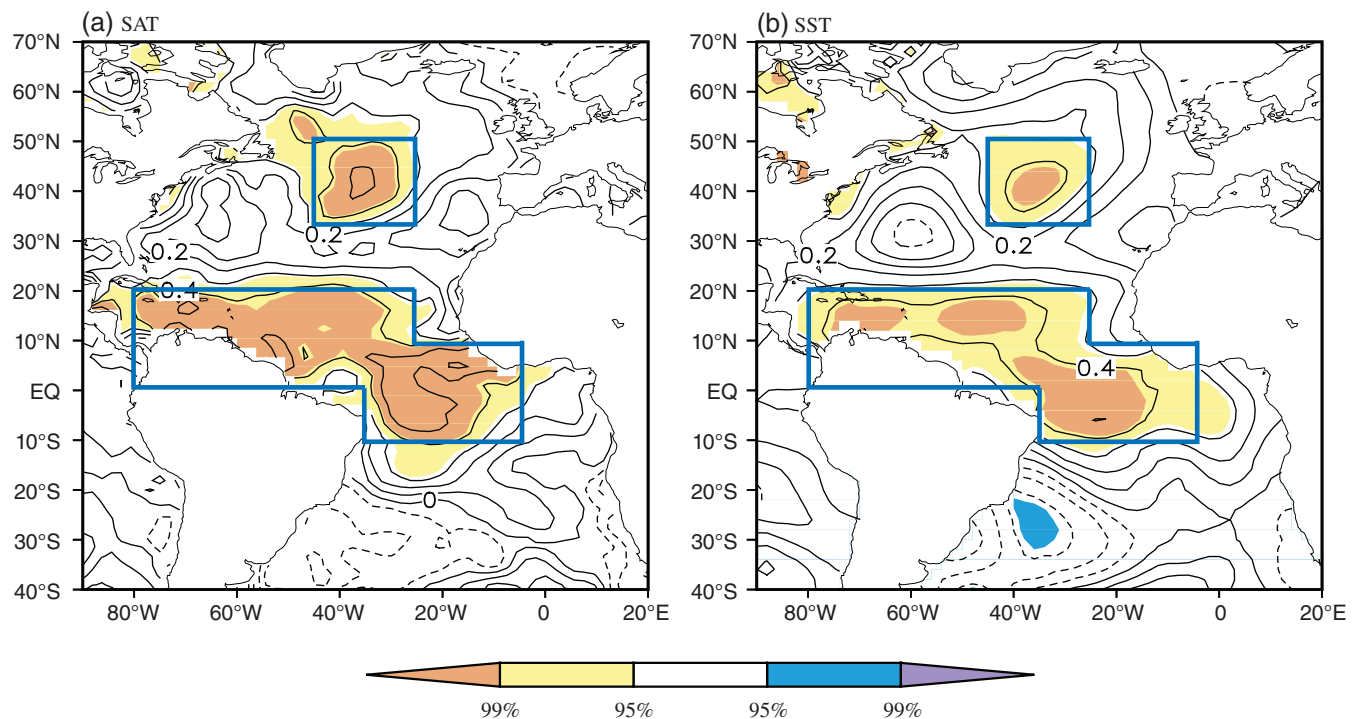

FIGURE 3 Distribution of correlation coefficients between the summer NEST index and simultaneous (a) SAT and (b) SST during the period 1980–2016. The blue boxes, from top to bottom, indicate the mid-latitude North Atlantic (45°–25°W, 33°–50°N) and tropical Atlantic (0°–20°N, 80°–25°W and 0°–10°N, 25°–5°W and 35°–5°W, 10°S–0°) regions, respectively. To focus on the characteristics of SAT over sea, the SAT over land has been removed in (a). Contours are drawn every 0.1. Shadings denote correlations significant at the 95% and 99% confidence levels as shown by the colour bars [Colour figure can be viewed at wileyonlinelibrary.com]
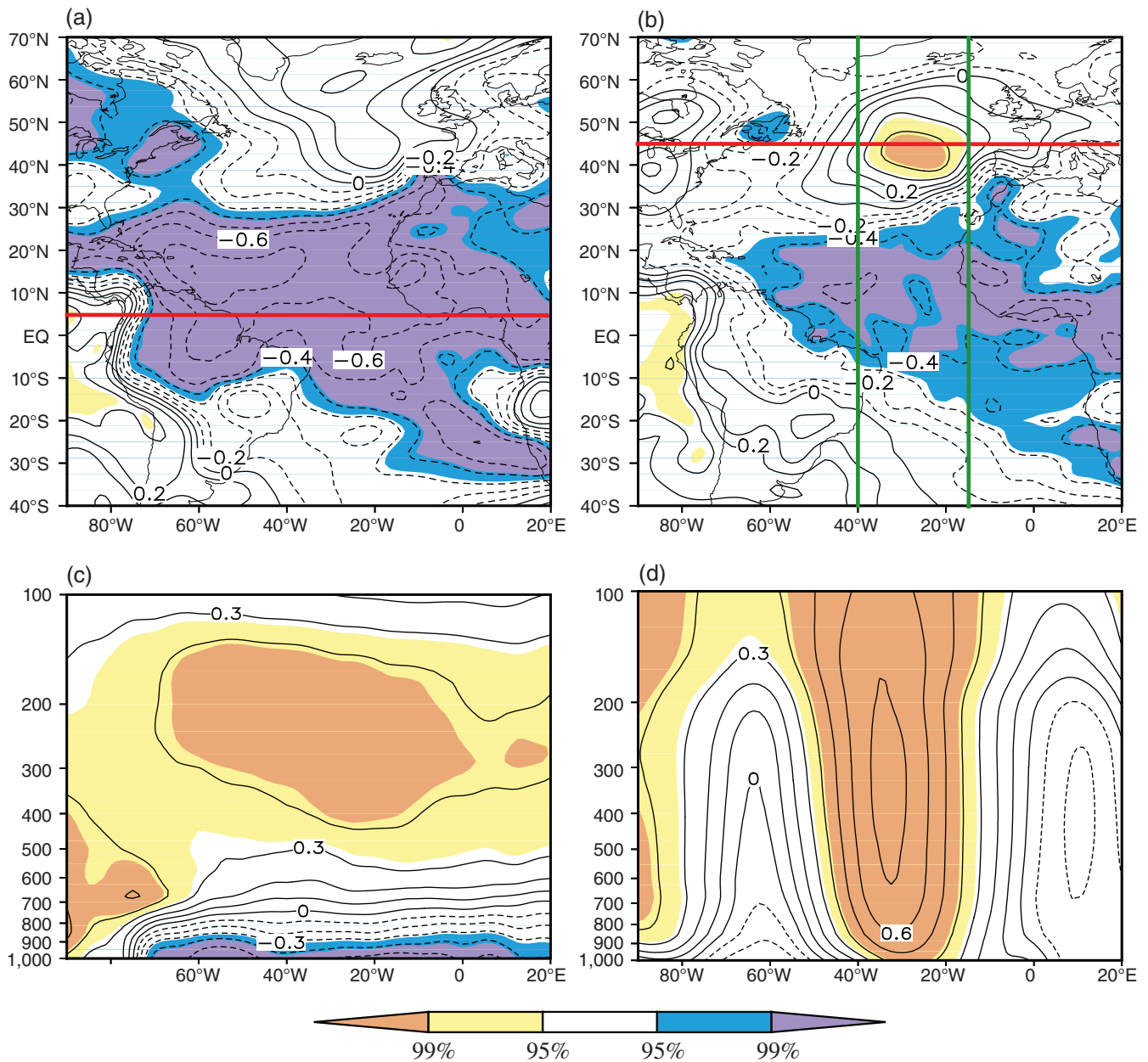
FIGURE 4 Correlation of summer 1,000-hPa geopotential heights with the summer (a) tropical Atlantic and (b) mid-latitude North Atlantic SAT indices during the period 1980–2016. (c) Correlation of summer geopotential heights with the summer tropical SAT index on a zonal–vertical cross section along 5°N [red line in (a)]. (d) As in (c) but for the correlation with the summer mid-latitude North Atlantic SAT index along 45°N [red line in (b)]. Contours are drawn every 0.1. Shadings denote correlations significant at the 95% and 99% confidence levels as shown by the colour bars. The two green lines cover a zone 40°–15°W, which is selected to draw Figure 5a [Colour figure can be viewed at wileyonlinelibrary.com]

the summer tropical Atlantic SAT index and simultaneous geopotential heights on a zonal–vertical cross section along 5°N (Figure 4c) further indicates that corresponding to warmer SAT over the tropical Atlantic region, surface low-pressure anomalies occur in the lower troposphere, while high-pressure anomalies appear in the upper troposphere. This baroclinic structure reflects deep convective activities, which are generally attributed to surface thermal forcing. This confirms the effect of

thermal anomalies over the tropical Atlantic region on the overlying atmospheric circulation anomalies, which is a prerequisite for the formation of the downstream wave train over Eurasia.

When warmer (cooler) SAT occur in the mid-latitude North Atlantic region, low-level higher (lower) pressure anomalies appear in situ (Figure 4b). Meanwhile, a deep high-pressure ridge appears corresponding to higher SAT over the mid-latitude North Atlantic region. This

correspondence can be clearly detected in the correlation between the summer mid-latitude North Atlantic SAT index and simultaneous geopotential heights on a zonal–vertical cross section along 45°N (Figure 4d). The 'warm SST–ridge' relationship over the extratropical Atlantic reflects the impact of atmosphere on the ocean (Zhao *et al.*, 2012). In short, the surface thermal anomalies over the mid-latitude North Atlantic region are merely a passive response to the overlying atmospheric circulation anomalies.

Additionally, the anomaly of net surface heat flux regressed upon the tropical (mid-latitude North) Atlantic SST index is 1.59 (−0.62) W·m^{-2}. This indicates that higher SST tends to supply (obtain) heat to (from) the atmosphere in the tropical (mid-latitude North) Atlantic region. This result also supports that the tropical Atlantic affects the overlying atmosphere through heating, but the mid-latitude North Atlantic does not. Therefore, this paper focuses on the effect of the thermal anomalies in the tropical Atlantic region on the summer NEST pattern.

Figure 5a presents anomalous vertical circulation and geopotential heights regressed upon the summer tropical Atlantic SAT index along a 40°W–15°W mean longitude-vertical cross section. The warmer tropical Atlantic stimulates an anomalous vertical circulation between the tropics and the mid- to high-latitude North Atlantic (Figure 5a). Specifically, air ascends over the tropical Atlantic (around 10°S–20°N), and then flows northwards in the upper troposphere, and finally descends and therefore leads to a deep high-pressure anomaly over the mid- to high-latitude North Atlantic (around 40°–60°N). This high-pressure anomaly may be responsible for warmer SST/SAT in the mid-latitude North Atlantic (Figure 3) through reducing upward motion/rainfall and increasing downward solar radiation reaching the Earth's surface. Meanwhile, this high-pressure anomaly can also be clearly seen in the upper troposphere over the mid- to high-latitude North Atlantic, featuring a downstream wave-like pattern over northern Eurasia (Figure 5b). Correspondingly, a positive–negative–positive wave train pattern of deep high-/low-pressure anomalies appears over
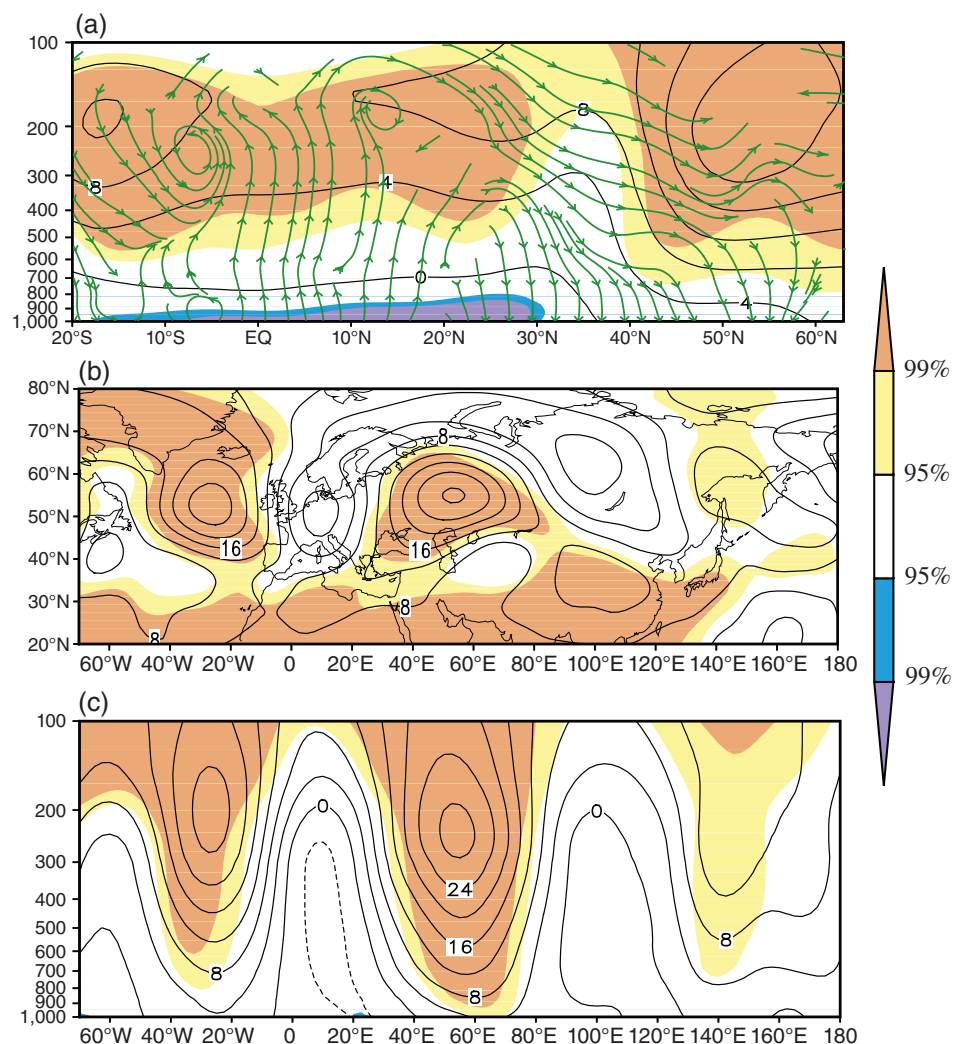

FIGURE 5 Summer geopotential height (units: gpm; contours and shading) and vertical circulation (green vectors) anomalies obtained by regression on the summer tropical Atlantic SAT index along a 40°–15°W mean longitude–vertical cross section (between the two green lines in Figure 4b). (b) Summer 200-hPa geopotential height anomalies (units: gpm) obtained by regression on the summer tropical Atlantic SAT index. (c) As in (b) but for the zonal–vertical cross section along 55°N. Contours are drawn every 4 gpm. Shadings denote geopotential anomalies significant at the 95% and 99% confidence levels as shown by the colour bars [Colour figure can be viewed at wileyonlinelibrary.com]

northern Eurasia (Figure 5c), which is in good agreement with the NEST-related circulation pattern (Figure 2b).

The impact of the summer thermal anomalies in the tropical Atlantic region on the simultaneous wave train pattern can be further demonstrated through the composite difference of the 200-hPa wave-activity fluxes between the years of the higher (1987, 1988, 1998, 2008, and 2010) and lower (1992, 1994, 1997, 2000, and 2004) tropical Atlantic SAT indices (Figure 6). Anomalous Rossby wave-activity fluxes (red arrows) propagate from the mid- to high-latitude North Atlantic to the FE region, accompanying anomalous wave-energy divergences (light shading) and convergences (dark shading) across the Eurasian continent along the path of Rossby wave propagation (Figure 6). The anomalous Rossby wave-activity fluxes at the 500-hPa level show a similar path (not shown). This path is also in good agreement with the Atlantic–Eurasian wave train pattern of geopotential height anomalies (Figure 5b,c). This further confirms that the summer SAT anomaly over the tropical Atlantic region can induce the positive–negative–positive geopotential height anomalies over northern Eurasia through a downstream dispersion of Rossby wave energy.

As a result of the aforementioned processes, the correlation between the summer tropical Atlantic SAT index and simultaneous SAT over northern Eurasia is positive over the EEWS and FE regions and negative over the BL region (Figure 7a). Such a distribution resembles the NEST pattern (Figure 1a). The summer tropical Atlantic SAT and NEST indices show a consistent variation, with a correlation coefficient of 0.59 during the period 1980–2016, significant at the 99.9% confidence level. Furthermore, the interannual components of the two time series, which are obtained using eight-year high-pass Lanczos filtering (Duchon, 1979), have a correlation coefficient of 0.51, significant at the 99% confidence level. For the interdecadal components (obtained using eight-year low-pass Lanczos filtering), the correlation coefficient is

0.76, significant at the 98% confidence level using the 10,000-time Monte Carlo test. The results reveal that a link between summer SAT over the tropical Atlantic region and simultaneous NEST pattern on both the interannual and interdecadal time scales.

4.2 | Precursory signals in the Atlantic Ocean and Eurasian land

4.2.1 | Effect of preceding rainfall and soil moisture anomalies around the BL

Relative to that in Figure 1a, the negative correlation around the BL region in Figure 7a is weaker and
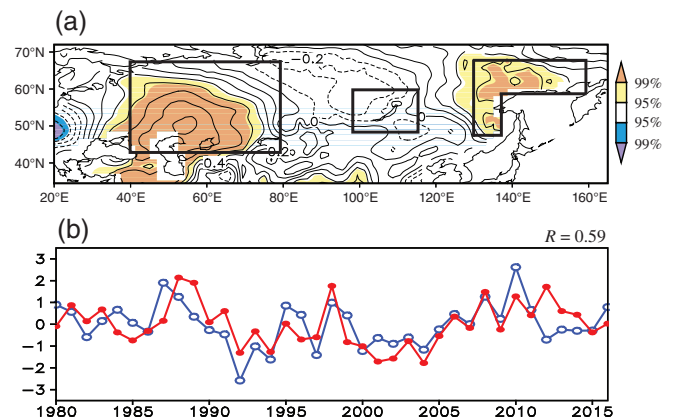
FIGURE 7 (a) Distribution of correlation coefficients between the summer tropical Atlantic SAT index and concurrent SAT during the period 1980–2016. The three black boxes are the same as those in Figure 1. Contours are drawn every 0.1. Shadings denote correlations significant at the 95% and 99% confidence levels as shown by the colour bars. (b) Normalized time series of the summer tropical Atlantic SAT (blue line) and NEST (red line) indices [Colour figure can be viewed at wileyonlinelibrary.com]
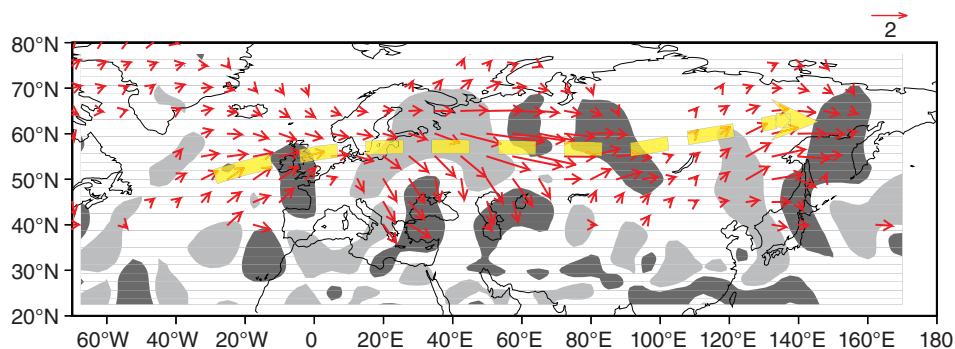
FIGURE 6 Composite difference in summer 200-hPa wave-activity fluxes (units: m^{-2} s^{-2}; red arrows) between years with high and low summer tropical Atlantic SAT indices (high minus low), in which the fluxes over the low latitudes have been removed. Light (dark) shading marks the regions where the divergences of wave-activity fluxes are greater (smaller) than 1.0×10^{-6} (-1.0×10^{-6}) m s^{-2}. The yellow thick dashed line with an arrow indicates the propagation pathway of Rossby waves [Colour figure can be viewed at wileyonlinelibrary.com]

nonsignificant though a similar NEST structure appears. Correspondingly, the tropical Atlantic SAT-related geopotential height anomalies around the BL region (Figure 5b,c) are remarkably weaker than those associated with the NEST (Figure 2). This implies that other factors may play a role in modulating atmospheric circulation and associated SAT anomalies over the BL region and accordingly affect the NEST pattern. Rainfall and related soil moisture anomalies can directly affect overlying atmospheric circulation. Moreover, the effect of rainfall and soil moisture anomalies can be considered as an important source of precursory signals for climate prediction in some areas since soil moisture has a good persistence/memory from several weeks to months (Entin *et al.*, 2000; Koster and Suarez, 2001; Douville *et al.*, 2006; Moon and Ha, 2019). Therefore, the contribution of rainfall and soil moisture anomalies should be investigated.

Correlation analysis reveals that the summer NEST is significantly and positively correlated with rainfall around the BL during the preceding May (Figure 8a). However, there are no clear signals of the rainfall anomalies in the earlier months (not shown). The BL rainfall index is defined as the area-mean rainfall averaged over the BL region (50°–58°N, 109°–117°E; see the black box in Figure 8a). The May BL rainfall index is significantly correlated with May–June mean soil moisture around the BL (Figure 8b), implying that more rainfall results in higher soil moisture around the BL in May, and the latter can maintain from May to June.

The higher soil moisture enhances the convective available potential energy through increasing the humidity of boundary layer air and accordingly facilitates local convection and rainfall (Betts *et al.*, 1996; Eltahir, 1998; Schär *et al.*, 1999). In turn, higher rainfall results in higher soil moisture during the ensuing period. As a result of the persistent soil moisture-rainfall interaction, more rainfall also appears around the BL during summer (Figure 8c) in correspondence to more rainfall (Figure 8a) and higher soil moisture during the preceding months (Figure 8b). Consistent with more convection/rainfall, deep low-pressure anomalies appear around the BL region during summer (Figure 9a,b), which contributes to negative SAT anomalies around the BL region (Figure 10a). The effect of rainfall and soil moisture anomalies around the BL may also modulate downstream atmospheric circulation (Figure 9a,b) and therefore result in positive SAT anomalies in the FE region (Figure 10a). Owing to the above processes, the May BL rainfall index is closely related to the summer NEST pattern, with a correlation coefficient of 0.45, significant at the 99% confidence level.
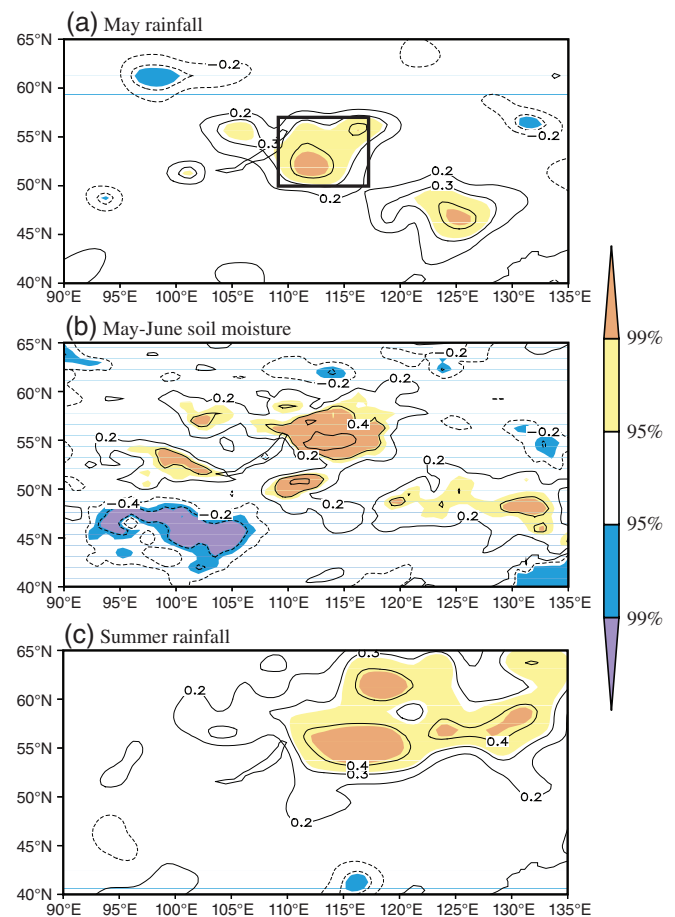

FIGURE 8 (a) Distribution of correlation coefficients between the summer NEST index and rainfall during the preceding May for the period 1980–2016. The black box represents the Baikal Lake (BL) region (50°–57°N, 109°–117°E) that is used to define the May BL rainfall index. (b) As in (a), but for that between the May BL rainfall index and May–June mean soil moisture. (c) As in (b), but for that between the May BL rainfall index and summer rainfall. Shadings denote correlations significant at the 95% and 99% confidence levels as shown by the colour bars [Colour figure can be viewed at wileyonlinelibrary.com]

4.2.2 | Effect of preceding thermal anomalies in the tropical Atlantic

The correlation between the summer NEST index and SAT/SST during the preceding May shows significant positive correlations in the tropical Atlantic (Figure 11a, b). In addition, the May tropical Atlantic SAT index, which is defined as the area-mean SAT averaged over the tropical Atlantic region (10°–25°N, 80°–25°W and 15°S–10°N, 35°–15°W) as shown in Figure 11a,b (the blue boxes), is significantly correlated with SST/SAT in the tropical Atlantic during the ensuing summer (Figure 11c, d). This indicates that the thermal anomalies in the tropical Atlantic can maintain from May to summer. To be
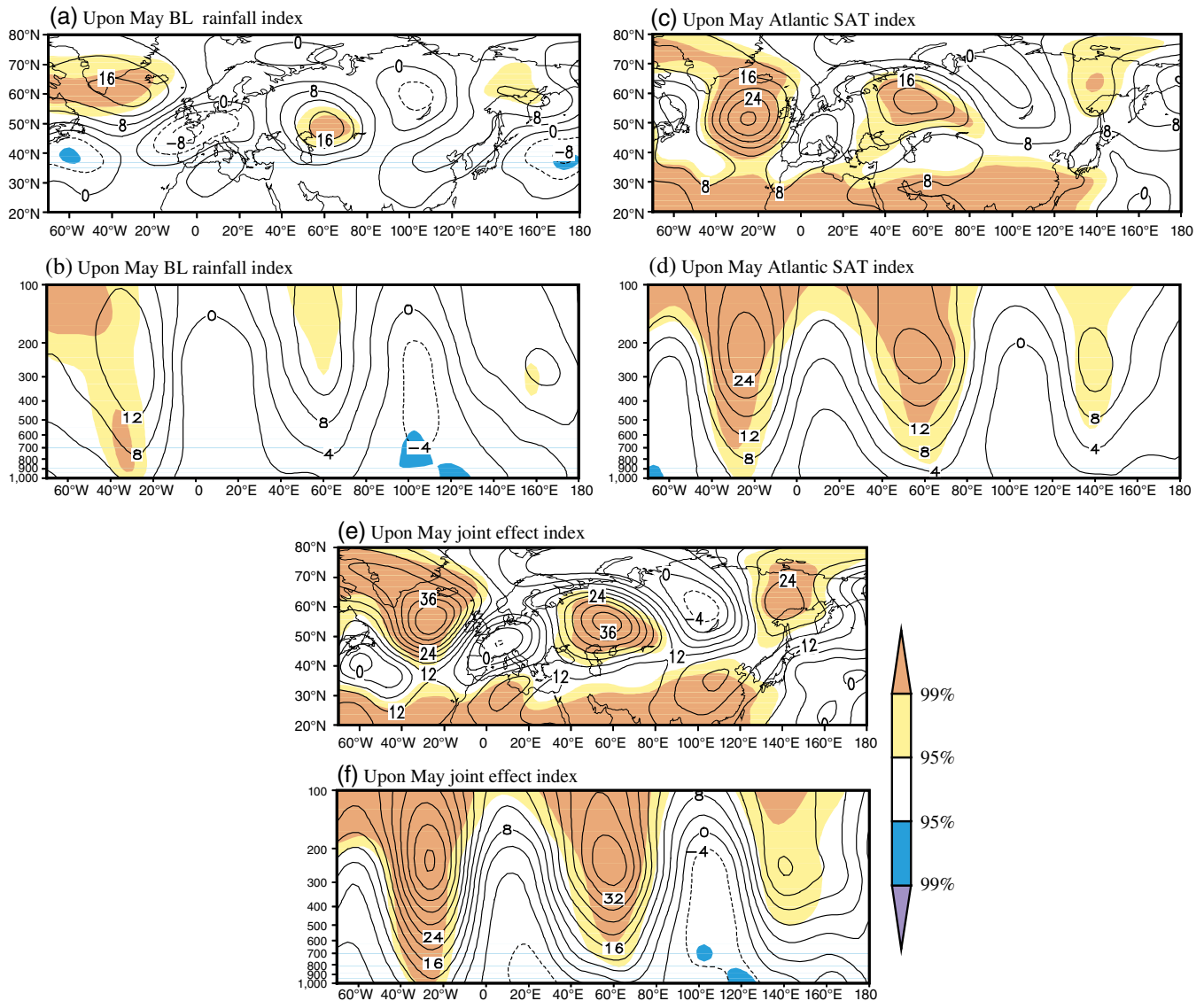
FIGURE 9 Summer 200-hPa geopotential height anomalies (units: gpm) obtained by regression upon the preceding May BL rainfall (a), tropical Atlantic SAT (c), and joint effect (e) indices, respectively. (b), (d), and (f) As in (a), (c), and (e), respectively, but for the zonal–vertical cross section along 55°N. Shadings denote geopotential height anomalies significant at the 95% and 99% confidence levels as shown by the colour bars [Colour figure can be viewed at wileyonlinelibrary.com]

consistent with the time of the BL rainfall signal, we explore the oceanic thermal signal in the preceding May. In fact, the preceding signal in the tropical Atlantic can be traced to the earlier months (not shown).

The thermal anomalies in the tropical Atlantic can persist from May to summer, and therefore cause downstream atmospheric circulation anomalies through a Rossby wave. This can be identified in summer geopotential height anomalies regressed upon the May tropical Atlantic SAT index (Figure 9c,d). Accompanying this wave-like pattern of geopotential height anomalies, a NEST anomaly appears over northern Eurasia (Figure 10b). Similar to the effect of the summer tropical Atlantic

thermal anomalies on atmospheric circulation (Figure 5b,c) and SAT (Figure 7a) anomalies, the May tropical Atlantic SAT-related low-pressure (negative SAT) anomalies around the BL are also weak and nonsignificant (see Figures 9c,d and 10b). This may be due to the absence of the preceding BL rainfall and soil moisture signals.

The correlation coefficient between the preceding May tropical Atlantic SAT and summer NEST indices is 0.51, significant at the 99% confidence level. This high correlation and the aforementioned physical processes reveal that the preceding May tropical Atlantic SAT is physically linked with and can be applied in predicting the summer NEST.

FIGURE 10 As in Figure 9a,c,e, but for SAT anomalies (units: °C) [Colour figure can be viewed at wileyonlinelibrary.com]
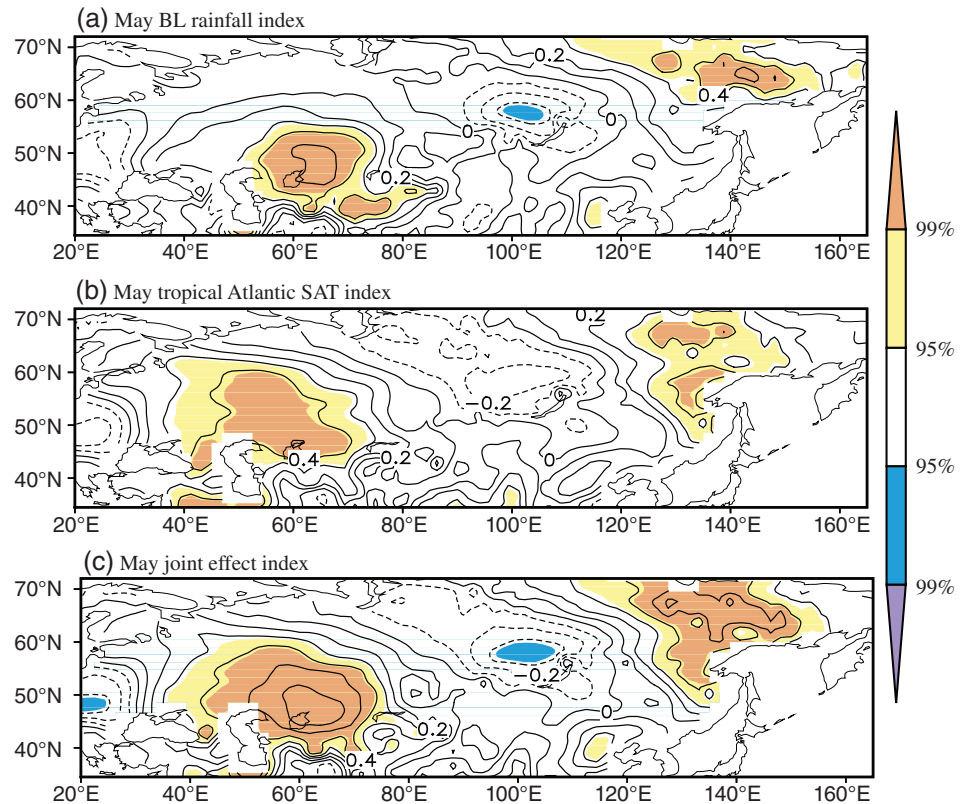
4.2.3 | Joint effect of preceding BL rainfall and tropical Atlantic thermal anomalies

The May BL rainfall index is independent of the simultaneous tropical Atlantic SAT index, with a nonsignificant correlation coefficient of 0.20. Using the linear fitting method (Hu *et al.*, 2012), we obtained the May individual BL rainfall (tropical Atlantic SAT) index after removing the effect of simultaneous tropical Atlantic SAT (BL rainfall). The correlation coefficient between the May individual BL rainfall (tropical Atlantic SAT) and summer NEST indices still reaches 0.36 (0.43), significant at the 95% (99%) confidence level. This further implies the independent effects of the two precursory signals on the summer NEST. Given the independence and effect of the two precursory signals, we established a linear regression model as follows.

$$I_{NEST} = 0.441 I_{Atlantic\text{-}SAT} + 0.363 I_{BL\text{-}rain},$$

in which I_{NEST}, $I_{\text{Atlantic - SAT}}$, and $I_{\text{BL - rain}}$ represent the normalized time series of the predicted summer NEST, May tropical Atlantic SAT, and May BL rain indices, respectively. The prediction skill of this model, measured by the correlation coefficient between the predicted and observational NEST indices, is 0.63 for the period 1980–2016, significant at the 99.9% confidence level. The root mean square error (RMSE) is 0.81, lower than that

(0.88/0.92) of the model using only the precursory signal of May tropical Atlantic SAT/BL rain. This indicates that the two precursory signals can provide higher prediction skill and stability than a signal one. Furthermore, the prediction skill of this model reaches 0.51 through the leave-three-out cross-validation, significant at the 99.8% confidence level. The aforementioned results suggest the applicability of the prediction model.

The right terms of this prediction model reflect the joint effect of the May tropical Atlantic SAT and BL rainfall with different weights. As such, the right terms can be referred to as the joint effect index of the two factors. Relative to the individual impacts of the two factors (Figure 9a–d), summer geopotential height anomalies regressed upon the May joint effect index (Figure 9e,f) show a clearer and more significant Rossby wave train from the Atlantic to the FE region, and therefore lead to a clearer NEST pattern during summer (Figure 10c). Using the ERA-interim reanalysis data, we further confirm the joint effect of the May tropical Atlantic SAT and BL rainfall on the summer atmospheric circulation and associated NEST variability (Figure 12).

5 | SUMMARY AND DISCUSSION

This study investigates the variability of summer SAT over northern Eurasia and its precursory signals in the
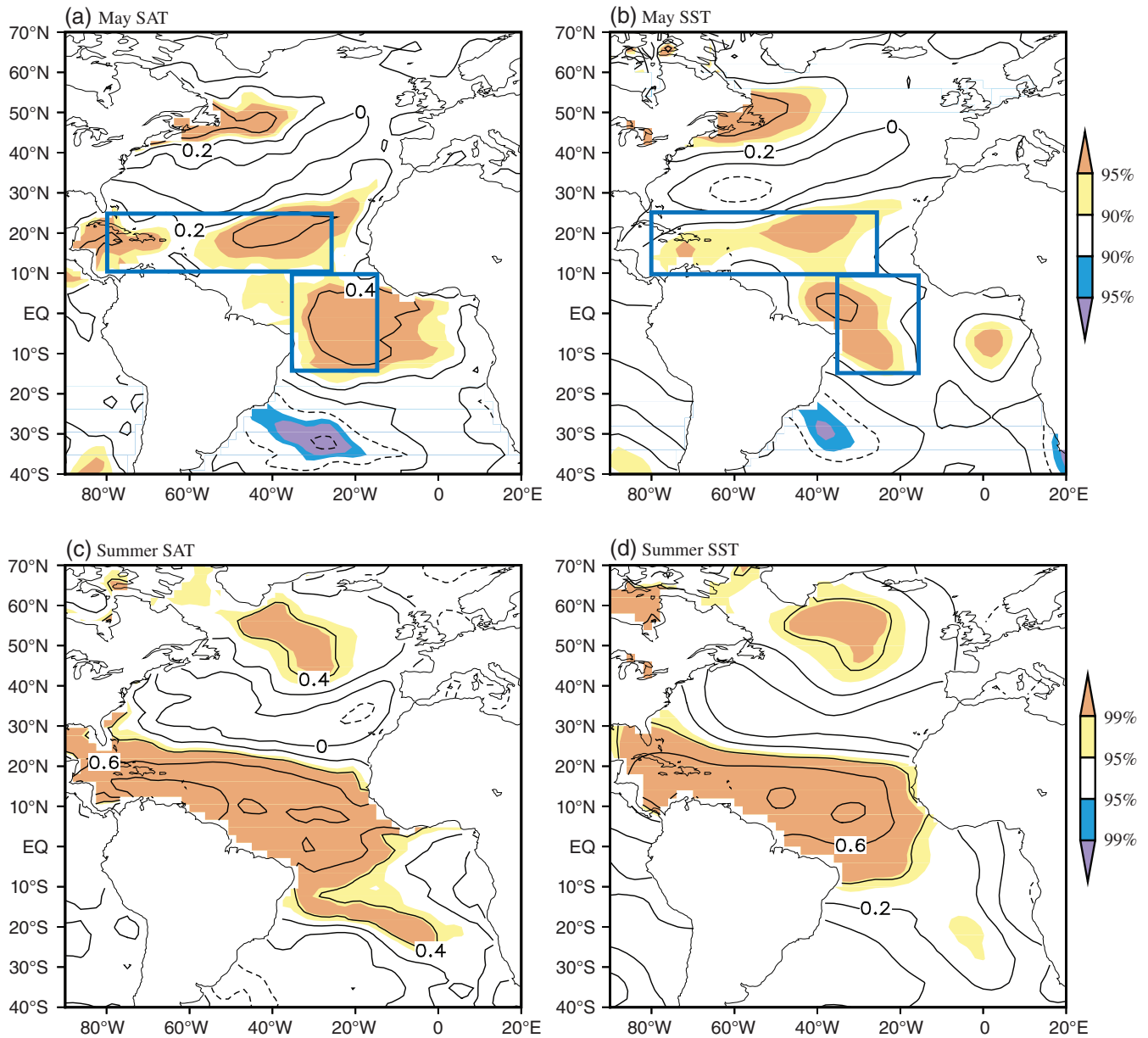
FIGURE 11 Distribution of correlation coefficients between the summer NEST index and preceding May (a) SAT and (b) SST during the period 1980–2016. Shadings denote correlations significant at the 90% and 95% confidence levels as shown by the colour bars. The blue boxes represent the tropical Atlantic region (10°–25°N, 80°–25°W and 15°S–10°N, 35°–15°W) that is used to the preceding May tropical Atlantic SAT index. (c) and (d) As in (a) and (b), but for that between the preceding May tropical Atlantic SAT index and summer (c) SAT and (d) SST. Shadings denote correlations significant at the 95% and 99% confidence levels as shown by the colour bars [Colour figure can be viewed at wileyonlinelibrary.com]

tropical Atlantic and northern Eurasia. The results show that the leading mode of summer SAT variations over northern Eurasia is characterized by a NEST pattern with same-sign SAT anomalies over the EEWS and FE regions, and opposite-sign SAT anomalies over the BL region. The summer NEST pattern is modulated by thermal (SAT-SST) anomalies in the tropical Atlantic and rainfall-soil moisture anomalies around the BL region during the preceding May.

The physical processes linking the abovementioned two precursory sea-land signals and the summer NEST pattern are summarized in Figure 13. The positive thermal anomalies in the tropical Atlantic maintain from May to summer and stimulate an anomalous longitude–vertical circulation between the tropics and the mid- to high-latitudes of the Atlantic Ocean, with anomalous upward motion over the tropical Atlantic region and anomalous downward motion and a related deep high-
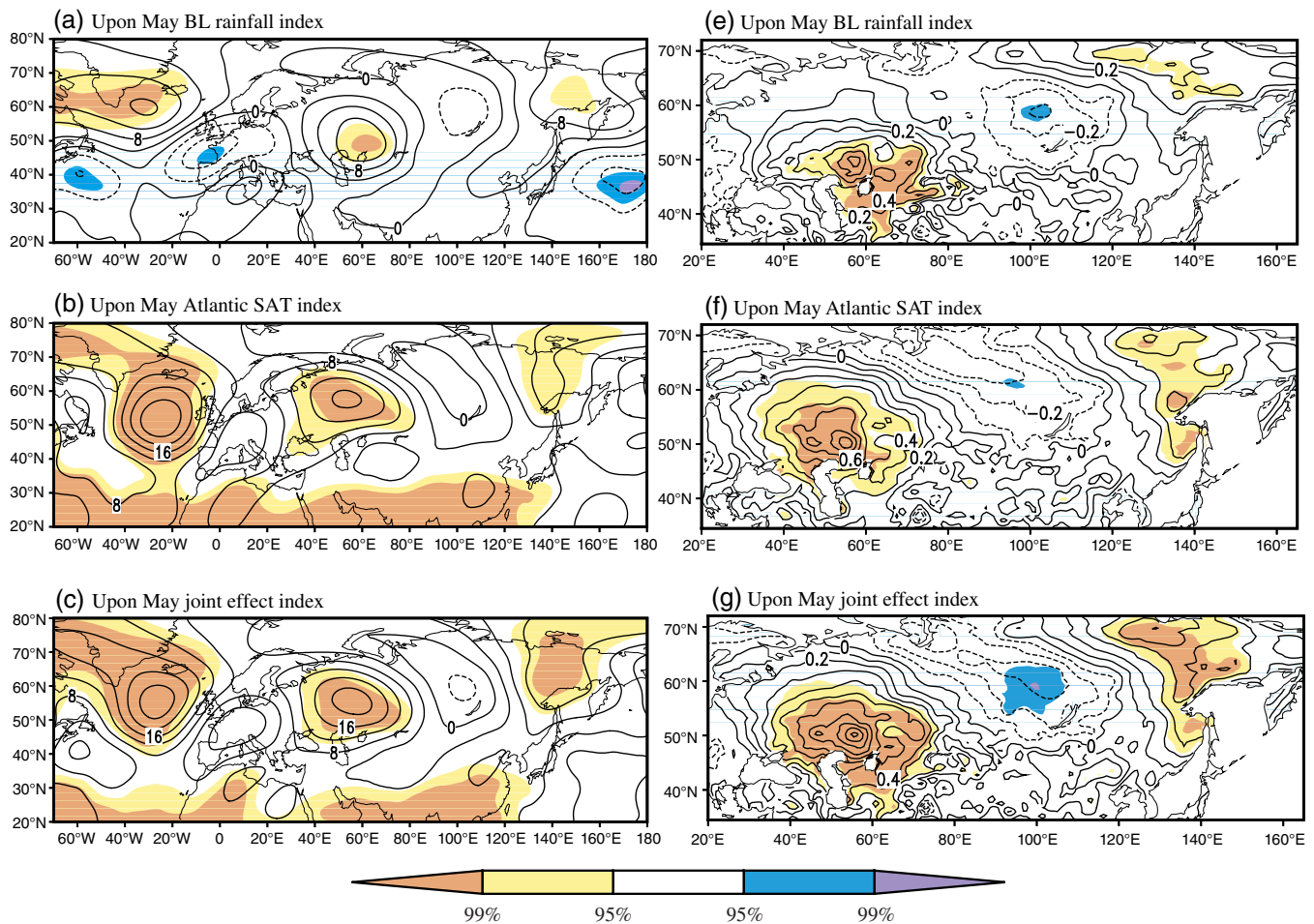
FIGURE 12 Summer 200-hPa geopotential height anomalies (units: gpm) obtained by regression upon the preceding May BL rainfall (a), tropical Atlantic SAT (b), and joint effect (c) indices, respectively. (e), (f), and (g) As in (a), (b), and (c), respectively, but for SAT anomalies (units: °C). All these figures are based on the ERA-interim reanalysis data. Shadings denote geopotential height anomalies significant at the 95% and 99% confidence levels as shown by the colour bars [Colour figure can be viewed at wileyonlinelibrary.com]

pressure anomaly over the mid- to high-latitude North Atlantic. The pressure anomaly over the mid- to high-latitude North Atlantic induces a downstream Rossby wave train across northern Eurasia. Accompanying this wave train, a positive–negative–positive pattern of height anomalies appears over northern Eurasia and therefore leads to a positive phase of the summer NEST pattern. Similarly, a negative phase of the summer NEST pattern can be attributed to the impact of negative thermal anomalies in the tropical Atlantic. Therefore, the summer NEST pattern is closely related to the preceding May tropical Atlantic SAT.

As summarized in Figure 13, May rainfall anomalies can adjust May–June soil moisture and eventually affect summer atmospheric circulation and convection/rainfall anomalies around the BL region through the 'memory' effect of soil moisture and the persistent soil moisture-rainfall interaction. Accordingly, the Rossby wave train from the BL to FE regions is modulated by the effect of

rainfall and soil moisture anomalies around the BL region, and so is the variability of the summer NEST. Due to this physical connection, the May BL rainfall index is remarkably correlated with the summer NEST.

Further analysis reveals that the joint effect of the two precursory signals can enhance the Rossby wave pattern and associated NEST pattern during summer. Moreover, the variability of May BL rainfall is independent of that of simultaneous tropical Atlantic SAT. Thus, a physics-based statistical prediction model of the summer NEST can be constructed using the two predictors. The prediction skill of this model reaches 0.51 (significant at the 99.8% confidence level) through the leave-three-out cross-validation.

Saeed *et al.* (2014) suggested that warm SSTAs in the subtropical Atlantic can lead to a positive circumglobal wave train (CGT) phase and consequently modulate precipitation over Europe. Following Saeed *et al.* (2011), the CGT index is defined as the PC associated with the EOF1
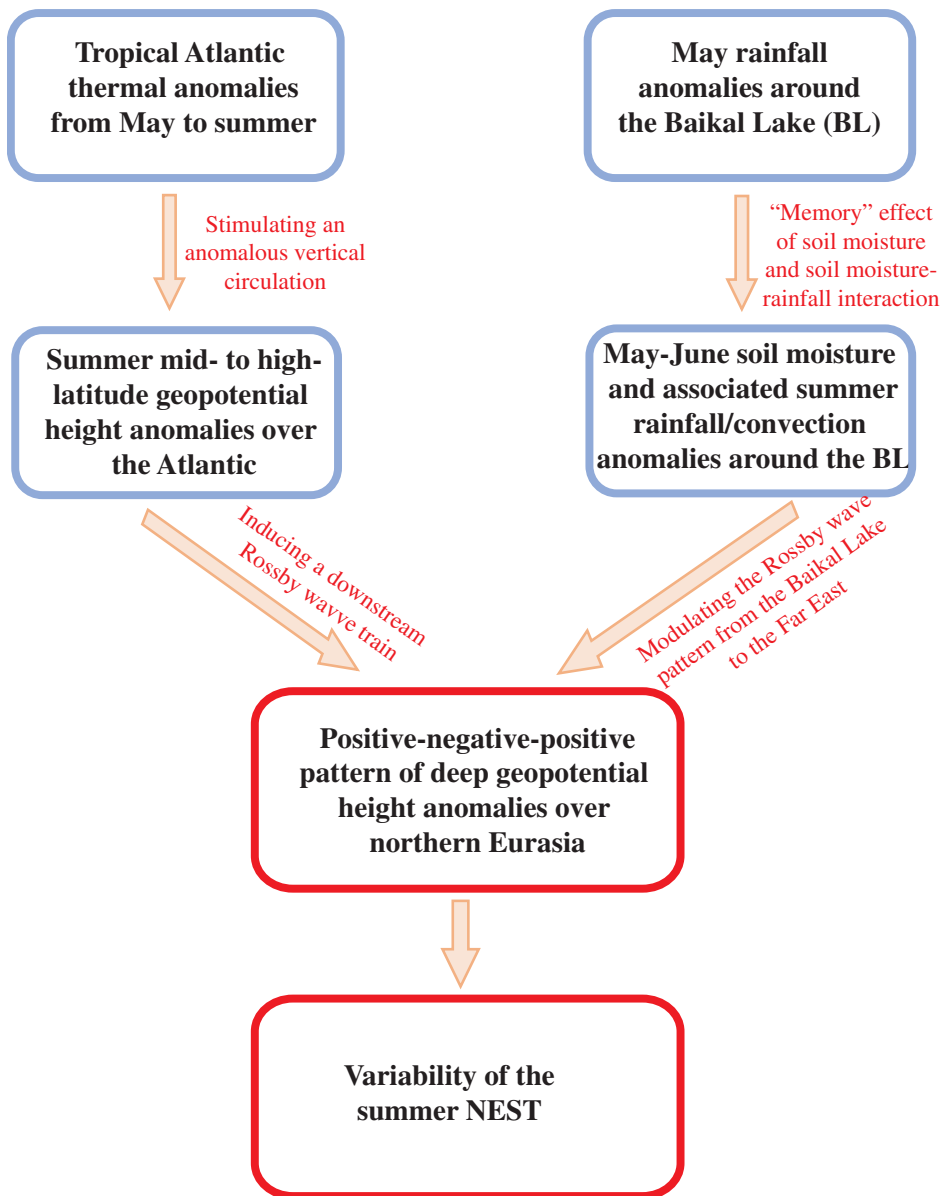
Tropical Atlantic thermal anomalies from May to summer

Stimulating an anomalous vertical circulation

Summer mid- to high-latitude geopotential height anomalies over the Atlantic

Inducing a downstream Rossby wave train

May rainfall anomalies around the Baikal Lake (BL)

"Memory" effect of soil moisture and soil moisture-rainfall interaction

May–June soil moisture and associated summer rainfall/convection anomalies around the BL

Modulating the Rossby wave pattern from the Baikal Lake to the Far East

Positive-negative-positive pattern of deep geopotential height anomalies over northern Eurasia

Variability of the summer NEST

FIGURE 13 Schematic diagram summarizing the processes linking the precursory sea-land signals during May and the variability of the NEST during summer [Colour figure can be viewed at wileyonlinelibrary.com]

of summer 200-hPa meridional wind anomalies over the domain (20°–80°N, 100°W–100°E). Summer 200-hPa geopotential height anomalies regressed upon the simultaneous CGT index show a wave train pattern from the Atlantic to the Okhotsk Sea via Eurasia, roughly similar to the NEST-related pattern except for a remarkably weaker anomaly around the FE region (not shown). Correspondingly, summer SAT anomalies regressed upon the simultaneous CGT index further show that the western part (i.e., the EEWS and BL regions), rather than the entire structure, of the NEST pattern may be related to the CGT (not shown). The CGT may play an important bridge role linking the previous SSTAs in the Atlantic Ocean to the western part of the summer NEST pattern though it cannot be directly used as a potential predictor of the summer NEST due to its poor cross-seasonal

persistence. The Atlantic SSTA-CGT-NEST physical link should be investigated in the future.

This study emphasizes the effect of the thermal conditions in the tropical Atlantic and rainfall/soil moisture anomalies around the BL region on the summer NEST pattern. The summer NEST variation may also be modulated by other oceanic and land external forcing. For example, the remote impact of the Arctic sea ice (Chen and Wu, 2018), thermal conditions over the Pacific (Sun *et al*., 2016), and the local land–air feedbacks of snow cover (Wu *et al*., 2014) and/or soil moisture anomalies over the Eurasian continent (Zhang and Dong, 2010; Fischer *et al*., 2012; Boé and Terray, 2014; Miralles *et al*., 2014; Whan *et al*., 2015) may regulate climate variability over different areas of Eurasia. In addition, atmospheric circulation patterns (such as the North Atlantic Oscillation, the Arctic Oscillation, and

the Scandinavia pattern) may affect climate variability over Eurasia (Chen *et al.*, 2015, 2018). Therefore, further studies are needed to investigate the potential implication of these atmospheric patterns in the prediction of the summer NEST pattern. For the variation of the summer NEST pattern, the individual effects of these factors, and their synergized contribution in conjunction with the effect of the two oceanic and land factors that we proposed in the present study, should be further explored in the future.

ACKNOWLEDGEMENTS

ORCID

Kejun He https://orcid.org/0000-0001-7662-9276
Ge Liu https://orcid.org/0000-0003-1408-7664
Renguang Wu https://orcid.org/0000-0003-4712-2251

REFERENCES

Barriopedra, D., Fischer, E.M., Luterbacher, J., Trigo, R.M. and Garcia-Herrera, R. (2011) The hot summer of 2010: redrawing the temperature record map of Europe. *Science*, 322, 220–224.

Beniston, M. (2004) The 2003 heat wave in Europe: a shape of things to come? An analysis based on Swiss climatological data and model simulations. *Geophysical Research Letters*, 31, L02202. https://doi.org/10.1029/2003GL018857.

Berrisford, P., Dee, D., Poli, P., Brugge, R., Fielding, K., Fuentes, M., … Simmons, A. (2011). The ERA-Interim archive: Version 2.0. Available online: https://www.ecmwf.int/node/8174.

Besag, J. and Clifford, P. (1989) Generalized Monte Carlo significance tests. *Biometrika*, 76, 633–642.

Betts, A.K., Ball, J.H., Beljaars, A.C.M., Miller, M.J. and Viterbo, P. A. (1996) The land surface-atmosphere interaction: a review based on observational and global modeling perspectives. *Journal of Geophysical Research*, 101(D3), 7209–7225.

Boé, J. and Terray, L. (2014) Land–sea contrast, soil-atmosphere and cloud temperature interactions: interplays and roles in future summer European climate change. *Climate Dynamics*, 42, 683–699.

Bueh, C. and Nakamura, H. (2007) Scandinavian pattern and its climatic impact. *Quarterly Journal of the Royal Meteorological Society*, 133, 2117–2131.

Cassou, C., Terray, L. and Phillips, A.S. (2005) Tropical Atlantic influence on European heat waves. *Journal of Climate*, 18, 2805–2811.

Chen, S. and Wu, R. (2017) Interdecadal changes in the relationship between interannual variations of spring North Atlantic SST and Eurasian surface air temperature. *Journal of Climate*, 30 (10), 3771–3787.

Chen, S. and Wu, R. (2018) Impacts of early autumn Arctic sea ice concentration on the subsequent spring Eurasian surface air temperature variations. *Climate Dynamics*, 51(7–8), 2532–2542.

Chen, S., Wu, R. and Chen, W. (2015) The changing relationship between interannual variations of the North Atlantic Oscillation and northern tropical Atlantic SST. *Journal of Climate*, 28, 485–504.

Chen, S., Wu, R. and Liu, Y. (2016) Dominant modes of interannual variability in Eurasian surface air temperature during boreal spring. *Journal of Climate*, 29, 1109–1125.

Chen, S., Wu, R., Song, L. and Chen, W. (2018) Combined influence of the Arctic oscillation and the Scandinavia pattern on spring surface air temperature variations over Eurasia. *Journal of Geophysical Research*, 123(17), 9410–9429.

D'Arrigo, R., Wilson, R. and Li, J. (2006) Increased Eurasian tropical temperature amplitude difference in recent centuries: implications for the Asian monsoon. *Geophysical Research Letters*, 33, L22706. https://doi.org/10.1029/2006GL027507.

Dee, D.P., Uppala, S.M., Simmons, A.J., Berrisford, P., Poli, P., Kobayashi, S., Andrae, U., Balmaseda, M.A., Balsamo, G., Bauer, P., Bechtold, P., Beljaars, A.C.M., van de Berg, L., Bidlot, J., Bormann, N., Delsol, C., Dragani, R., Fuentes, M., Geer, A.J., Haimberger, L., Healy, S.B., Hersbach, H., Hólm, E. V., Isaksen, L., Kållberg, P., Köhler, M., Matricardi, M., McNally, A.P., Monge-Sanz, B.M., Morcrette, J.J., Park, B.K., Peubey, C., de Rosnay, P., Tavolato, C., Thépaut, J.N. and Vitart, F. (2011) The ERA-interim reanalysis: configuration and performance of the data assimilation system. *Quarterly Journal of the Royal Meteorological Society*, 137, 553–597.

Douville, H., Conil, S., Tyteca, S. and Voldoire, A. (2006) Soil moisture memory and West African monsoon predictability: artefact or reality? *Climate Dynamics*, 28, 723–742.

Duchon, C.E. (1979) Lanczos filtering in one and two dimensions. *Journal of Applied Meteorology and Climatology*, 18, 1016–1022.

Ehsan, M.A., Kucharski, F., Almazroui, M., Ismail, M. and Tippett, M.K. (2019) Potential predictability of Arabian peninsula summer surface air temperature in the North American multimodel ensemble. *Climate Dynamics*, 53, 4249–4266.

Ehsan, M.A., Nicolì, D., Kucharski, F., Almazroui, M., Tippett, M. K., Bellucci, A., Ruggieri, P. and Kang, I. (2020) Atlantic Ocean influence on Middle East summer surface air temperature. *Climate and Atmospheric Science*, 3, 5. https://doi.org/10.1038/s41612-020-0109-1.

Ehsan, M.A., Tippett, M.K., Almazroui, M., Ismail, M., Yousef, A., Kucharski, F., Omar, M., Hussein, M. and Alkhalaf, A.A. (2017) Skill and predictability in multimodel ensemble forecasts for northern hemisphere regions with dominant winter precipitation. *Climate Dynamics*, 48, 3309–3324.

Eltahir, E.A.B. (1998) A soil moisture-rainfall feedback mechanism. Part I: Theory and observations. *Water Resources Research*, 34, 765–776.

Entin, J.K., Robock, A., Vinnikov, K.Y., Hollinger, S.E., Liu, S. and Namkhai, A. (2000) Temporal and spatial scales of observed soil moisture variations in the extratropics. *Journal of Geophysical Research*, 105, 11865–11877.

Fang, X., Wang, Y. and Zhu, X. (2005) Change of cool summer hazard under an adaptation behavior to the climate warming in Heilongjiang Province, Northeast China. *Geographical Research* (in Chinese), 24, 664–672.

Feudale, L. and Shukla, J. (2011a) Influence of sea surface temperature on the European heat wave of 2003 summer. Part I: an observational study. *Climate Dynamics*, 36, 1691–1703.

Feudale, L. and Shukla, J. (2011b) Influence of sea surface temperature on the European heat wave of 2003 summer. Part II: a modeling study. *Climate Dynamics*, 36, 1705–1715.

Fischer, E.M., Rajczak, J. and Schär, C. (2012) Changes in European summer temperature variability revisited. *Geophysical Research Letters*, 39, L19702. https://doi.org/10.1029/2012GL052730.

Gao, M., Wang, B., Yang, J. and Dong, W. (2018) Are peak sultry heat wave days over the Yangtze-Huaihe River basin predictable? *Journal of Climate*, 31, 2185–2196.

Goswami, B.N., Madhusoodanan, M.S., Neema, C.P. and Sengupta, D. (2006) A physical mechanism for North Atlantic SST influence on the Indian summer monsoon. *Geophysical Research Letters*, 33, L02706. https://doi.org/10.1029/2005GL024803.

Hu, M., Gong, D., Wang, L., Zhou, T. and Zhang, Z. (2012) Possible influence of January-March Arctic oscillation on the convection of tropical North Pacific and North Atlantic. *Acta Meteorologica Sinica* (in Chinese), 70(3), 479–491.

Huang, B., Thorne, P., Smith, T., Liu, W., Lawrimore, J., Banzon, V., Zhang, H., Peterson, T. and Menne, M. (2015) Further exploring and quantifying uncertainties for extended reconstructed sea surface temperature (ERSST) version 4 (v4). *Journal of Climate*, 29, 3119–3142.

Kalnay, E., Kanamitsu, M., Kistler, R., Collins, W., Deaven, D., Gandin, L., Iredell, M., Saha, S., White, G., Woollen, J., Zhu, Y., Leetmaa, A., Reynolds, B., Chelliah, M., Ebisuzaki, W., Higgins, W., Janowiak, J., Mo, K.C., Ropelewski, C., Wang, J., Jenne, R. and Joseph, D. (1996) The NCEP/NCAR 40-year reanalysis project. *Bulletin of the American Meteorological Society*, 77, 437–471.

Koster, R.D. and Suarez, M.J. (2001) Soil moisture memory in climate models. *Journal of Hydrometeorology*, 2, 558–570.

Krishnamurthy, L. and Krishnamurthy, V. (2016) Teleconnections of Indian monsoon rainfall with AMO and Atlantic tripole. *Climate Dynamics*, 46, 2269–2285.

Kundu, P.K. and Allen, J.S. (1976) Some three-dimensional characteristics of low-frequency current fluctuations near the Oregon coast. *Journal of Physical Oceanography*, 6, 181–199.

Li, S., Jing, Y. and Luo, F. (2015) The potential connection between China surface air temperature and the Atlantic multidecadal oscillation (AMO) in the pre-industrial period. *Science China Earth Sciences*, 58, 1814–1826.

Li, S., Perlwitz, J., Quan, X. and Hoerling, M.P. (2008) Modelling the influence of North Atlantic multidecadal warmth on the Indian summer rainfall. *Geophysical Research Letters*, 35, L05804. https://doi.org/10.1029/2007GL032901.

Liu, G., Ji, L. and Wu, R. (2012) An east-west SST anomaly pattern in the midlatitude North Atlantic Ocean associated with winter precipitation variability over eastern China. *Journal of Geophysical Research*, 117, D15104. https://doi.org/10.1029/2012JD017960.

Liu, X. and Yanai, M. (2001) Relationship between the Indian monsoon rainfall and the tropospheric temperature over the Eurasian continent. *Quarterly Journal of the Royal Meteorological Society*, 127, 909–937.

Lu, R., Dong, B. and Ding, H. (2006) Impact of the Atlantic multidecadal oscillation on the Asian summer monsoon. *Geophysical Research Letters*, 33, L24701. https://doi.org/10.1029/2006GL027655.

Ma, S., Xi, Z. and Wang, Q. (2003) Risk evaluation of cold damage to corn in Northeast China. *Journal of Natural Disasters* (in Chinese), 12, 137–141.

Michaelsen, J. (1987) Cross-validation in statistical climate forecast models. *Journal of Applied Meteorology*, 26, 1589–1600.

Miralles, D.G., Teuling, A.J. and Van Heerwaarden, C.C. (2014) Mega-heatwave temperatures due to combined soil desiccation and atmospheric heat accumulation. *Nature Geoscience*, 7, 345–349.

Moon, S. and Ha, K.J. (2019) Early Indian summer monsoon onset driven by low soil moisture in the Iranian Desert. *Geophysical Research Letters*, 46, 10568–10577. https://doi.org/10.1029/2019GL084520.

Obukhov, A.M. (1947) Statistically homogeneous fields on a sphere. *Uspethi Mathematicheskikh Nauk*, 2, 196–198.

Saeed, S., Lipzig, V.N., Müller, W.A., Saeed, F. and Zanchettin, D. (2014) Influence of the circumglobal wave-train on European summer precipitation. *Climate Dynamics*, 43, 503–515.

Saeed, S., Müller, W.A., Hagemann, S. and Jacob, D. (2011) Circumglobal wave train and the summer monsoon over northwestern India and Pakistan: the explicit role of the surface heat low. *Climate Dynamics*, 37, 1045–1060.

Schär, C.D., Beyerle, L.U. and Heise, E. (1999) The soil-precipitation feedback: a process study with a regional climate model. *Journal of Climate*, 12(3), 722–741.

Sedláček, J., Martius, O. and Knutti, R. (2011) Influence of subtropical and polar sea-surface temperature anomalies on temperatures in Eurasia. *Geophysical Research Letters*, 38, L12803. https://doi.org/10.1029/2011GL047764.

Stott, P.A., Stone, D.A. and Allen, M.R. (2004) Human contribution to the European heatwave of 2003. *Nature*, 432, 610–614.

Sun, C., Li, J. and Ding, R. (2016) Strengthening relationship between ENSO and western Russian summer surface temperature. *Geophysical Research Letters*, 43, 843–851.

Sun, J. (2014) Record-breaking SST over mid-North Atlantic and extreme high temperature over the Jianghuai-Jiangnan region of China in 2013. *Chinese Science Bulletin*, 59, 3465–3470.

Sutton, R.T. and Dong, B. (2012) Atlantic Ocean influence on a shift in European climate in the 1990s. *Nature Geoscience*, 5, 788–792.

Sutton, R.T. and Hodson, D.L.R. (2005) Atlantic Ocean forcing of North American and European summer climate. *Science*, 309, 115–118.

Sutton, R.T. and Hodson, D.L.R. (2007) Climate response to basin-scale warming and cooling of the North Atlantic Ocean. *Journal of Climate*, 20, 891–907.

Takaya, K. and Nakamura, H. (1997) A formulation of a wave-activity flux for stationary Rossby waves on a zonally varying basic flow. *Geophysical Research Letters*, 24, 2985–2988.

Takaya, K. and Nakamura, H. (2001) A formulation of a phase-independent wave-activity flux for stationary and migratory quasi-geostrophic eddies on a zonally varying basic flow. *Journal of the Atmospheric Sciences*, 58, 608–627.

Tippett, M.K. (2004) Measuring the potential utility of seasonal climate predictions. *Geophysical Research Letters*, 31, L22201. https://doi.org/10.1029/2004GL021575.

Wang, H., Liu, G. and Chen, J. (2017) Contribution of the tropical western Atlantic thermal conditions during the preceding winter to summer temperature anomalies over the lower reaches of the Yangtze River basin–Jiangnan region. *International Journal of Climatology*, 37, 4631–4642. https://doi.org/10.1002/joc.5111.

Whan, K., Zscheischler, J., Orth, R., Shongwe, M., Rahimi, M., Asare, E.O. and Seneviratne, S.L. (2015) Impact of soil moisture on extreme maximum temperatures in Europe. *Weather and Climate Extremes*, 9, 57–67.

Wu, R. and Chen, S. (2020) What leads to persisting surface air temperature anomalies from winter to following spring over the mid-high latitude Eurasia? *Journal of Climate*, 33, 5861–5883. https://doi.org/10.1175/JCLI-D-19-0819.1.

Wu, R., Liu, G. and Zhao, P. (2014) Contrasting Eurasian spring and summer climate anomalies associated with western and eastern Eurasian spring snow cover changes. *Journal of Geophysical Research – Atmospheres*, 119, 7410–7424.

Wu, R., Yang, S., Liu, S., Sun, L., Lian, Y. and Gao, Z. (2010) Changes in the relationship between northeast China summer temperature and ENSO. *Journal of Geophysical Research*, 115, D21107. https://doi.org/10.1029/2010JD014422.

Wu, R., Yang, S., Liu, S., Sun, L., Lian, Y. and Gao, Z. (2011) Northeast China summer temperature and North Atlantic SST. *Journal of Geophysical Research*, 116, D16116. https://doi.org/10.1029/2011JD015779.

Wu, Z., Wang, B., Li, J. and Jin, F. (2009) An empirical seasonal prediction model of the east Asian summer monsoon using ENSO and NAO. *Journal of Geophysical Research*, 114, D18120. https://doi.org/10.1029/2009JD011733.

Xie, P. and Arkin, P.A. (1997) Global precipitation: a 17-year monthly analysis based on gauge observations, satellite estimates, and numerical model outputs. *Bulletin of the American Meteorological Society*, 78, 2539–2558.

Yue, X., Liu, G., Chen, J. and Zhou, C. (2020) Synergistic regulation of the interdecadal variability in summer precipitation over the Tianshan mountains by sea surface temperature anomalies in the high-latitude Northwest Atlantic Ocean and the Mediterranean. *Atmospheric Research*, 233, 104717. https://doi.org/10.1016/j.atmosres.2019.104717.

Zhang, J. and Dong, W. (2010) Soil moisture influence on summertime surface air temperature over East Asia. *Theoretical and Applied Climatology*, 100, 221–226.

Zhao, P., Yang, S., Wu, R., Wen, Z., Chen, J. and Wang, H. (2012) Asian origin of interannual variations of summer climate over the extratropical North Atlantic Ocean. *Journal of Climate*, 25, 6594–6609.

Zuo, J., Li, W., Sun, C., Xu, L. and Ren, H. (2013) Impact of the North Atlantic sea surface temperature tripole on the East Asian summer monsoon. *Advances in Atmospheric Sciences*, 30, 1173–1186.